arXiv:2410.03801v3 [cs.LG] 17 Mar 2025

P1-KAN: AN EFFECTIVE KOLMOGOROV-ARNOLD NETWORK WITH APPLICATION TO HYDRAULIC VALLEY OPTIMIZATION

XAVIER WARIN

Abstract. A new Kolmogorov-Arnold network (KAN) is proposed to approximate potentially irregular functions in high dimensions. We provide error bounds for this approximation, assuming that the Kolmogorov-Arnold expansion functions are sufficiently smooth. When the function is only continuous, we also provide universal approximation theorems. We show that it outperforms multilayer perceptrons in terms of accuracy and convergence speed. We also compare it with several proposed KAN networks: it outperforms all networks for irregular functions and achieves similar accuracy to the original spline-based KAN network for smooth functions. Finally, we compare some of the KAN networks in optimizing a French hydraulic valley.

1. Introduction

Kolmogorov-Arnold Networks [18], based on the Arnold-Kolmogorov representation theorem, have recently been proposed as an alternative to multilayer perceptrons for approximating functions in high dimensions. Arnold and Kolmogorov showed long ago [14] that a multivariate continuous smooth function f on a bounded domain can be written as a finite composition of the sum of continuous functions of a single variable. More precisely, if f is smooth on $[0,1]^n$, then

$$f(x) = \sum_{i=1}^{2n+1} \psi_i \left(\sum_{j=1}^{n} \Phi_{i,j}(x_j) \right), \tag{1}$$

where $\Phi_{i,j} : [0,1] \longrightarrow \mathbb{R}$ and $\psi_i : \mathbb{R} \longrightarrow \mathbb{R}$.
As the 1D functions can be very irregular or even fractal, it has been shown that they may not be learnable in practice [10, 19]. To overcome this limitation, [18] propose to extend this representation. First, they propose not to stick to $2n+1$ terms in the outer sum in (1) and to define a KAN l^{th} layer as an operator $\psi^l_{m,q}$ from $[0,1]^m$ to $\mathbb{R}^q$:

$$(\psi^l_{m,q}(x))_k = \sum_{j=1}^{m} \Phi_{l,k,j}(x_j), \text{ for } k = 1, \dots, q. \tag{2}$$

Second, by stacking the layers, i.e., composing the operator ψ^l, they define the KAN operator from $[0,1]^m$ to $\mathbb{R}^d$:

$$K(x) = (\psi^L_{n_{L-1},d} \circ \psi^{L-1}_{n_{L-2},n_{L-1}} \circ \dots \circ \psi^1_{n_0,n_1} \circ \psi^0_{m,n_0})(x)$$

Since all ψ functions are one-dimensional, many classical methods are available to propose an easy-to-implement approximation. In their proposed implementation, [18] use B-splines (see for example [5]) associated with the SILU activation function to approximate the ψ function: the spline coefficients and the multiplicative coefficient of the SILU function are learned using a classical stochastic gradient algorithm as done with MLPs.
This network has been rapidly tested, replacing MLPs in transformers [29] for example, and in various fields:

the medical sector in [13], vision [6, 16], time series [26]. Strengths and weaknesses of this approach compared to MLPs are discussed in [30] and, depending on its use, its superiority to MLPs is not always obvious [22, 15]. Following this first article, different evolutions of this architecture are proposed to address different problems: [7] proposes an evolution of the algorithm to replace LSTM in time series, [28] for Graph Collaborative Filtering, [3] for convolutional networks, [1] in mechanics.
The original spline-based algorithm has several drawbacks. The first disadvantage of this approach is that the spline approximation is expensive, at least in the original algorithm proposed. The second is that the output of a layer may not be in the grid initially chosen for the following layer. Finally, since the Kolmogorov representation theorem may involve a very irregular function, one may wonder whether it is interesting to use a rather high-order approximation such as a spline.
To address the first point, many other approximations based on classical numerical analysis have been proposed using: wavelets [4], radial basis [17, 25] which reduces the computation time by 3, Chebyshev polynomials [24] and many others. An interesting representation that leads to a very effective layer is the ReLU-KAN [20] [23], which is based only on the ReLU function, matrix addition and multiplication, and divides the computation time by 20.
To address the second point, some use a sigmoid activation function [24] to obtain an output in the range $[0, 1]$, but this approach is clearly very ineffective. Others attempt to adapt the support of the basis functions by trying to learn them [18], but this adaptation often fails.
Concerned by the possibility of KANs to approximate high-dimensional functions, especially for stochastic optimization purposes in [8],[27], we have developed the P1-KAN network, borrowing some interesting features from the ReLU-KAN, but clearly defining the support of the layer function and avoiding the network adaptation proposed in [18]. In the first part of the article, we describe our architecture and we give error bounds assuming that the functions in the expansion (1) are smooth enough. We also provide universal approximation theorems to deal with the general case of continuous functions. In the second part, we compare it with MLPs, Spline-KAN, Radial basis KAN, and ReLU-KAN on function approximation using either smooth or very irregular functions in different dimensions. Finally, we test the Spline-KAN and the P1-KAN to optimize a French hydraulic valley, comparing them with classical perceptrons.

2. The P1-KAN Networks

We will first explain the main features of the method, and then go into detail about the algorithm and why P1-KAN is different from other KAN networks.

2.1. **The P1-KAN Layers.**

The first possible layer uses a regular grid, while the second one uses a grid adapting to the data.

2.1.1. *The P1-KAN Layer with a Regular Lattice.*

We assume that layer l is an operator with support $G^l = (\underline{x}^l, \bar{x}^l) \in \mathbb{R}^{d_0 \times 2}$ and with values in $\mathbb{R}^{d_1}$. As for the classical KAN layers, a number of meshes per direction P (assumed constant per layer to simplify the notations) are used to discretize $[\underline{x}^l_1, \bar{x}^l_1] \times \ldots \times [\underline{x}^l_{d_0}, \bar{x}^l_{d_0}]$, giving the mesh vertices $(\hat{x}^l_{j,p})_{1 \leq p \leq P-1}$ in $]\underline{x}^l_j, \bar{x}^l_j[$ for $j = 1, \ldots, d_0$. Set $\hat{x}^l_{j,0} = \underline{x}^l_j$, $\hat{x}^l_{j,P} = \bar{x}^l_j$, the function $\Phi_{l,k,j}$ in (2) is defined using a P1 finite element method (see figure 1): for $x \in [\underline{x}^l_j, \bar{x}^l_j]$,

$$\Phi_{l,k,j}(x) = \sum_{p=0}^{P} a^{l,k,j}_p \Psi^{l,j}_p(x)$$

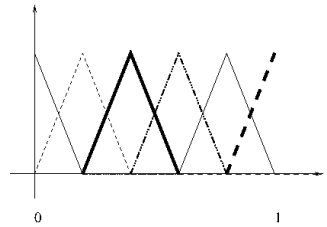

FIGURE 1. Uniform P_1 basis functions on $[0,1]$ with $P=5$.

where $(a_p^{l,k,j})_{p=0,P}$ are trainable variables and $(\Psi_p^{l,j})_{p=0,P}$ is the basis of the shape function $\Psi_p^{l,j}$ with compact support in each interval $[\hat{x}_{j,p-1}^l, \hat{x}_{j,p+1}^l]$ for $p=1,\dots,P-1$ and defined as:

$$\Psi_p^{l,j}(x) = \begin{cases} \frac{x-\hat{x}_{j,p-1}^l}{\hat{x}_{j,p}^l-\hat{x}_{j,p-1}^l} & x \in [\hat{x}_{j,p-1}^l, \hat{x}_{j,p}^l] \\ \frac{\hat{x}_{j,p+1}^l-x}{\hat{x}_{j,p+1}^l-\hat{x}_{j,p}^l} & x \in [\hat{x}_{j,p}^l, \hat{x}_{j,p+1}^l] \end{cases}$$
$$\text{such that } \Psi_p^{l,j}(\hat{x}_{j,q}^l) = \delta_{q,p},$$

for $p=1,\dots,P-1$. Similarly, $\Psi_0^{l,j}$ (or $\Psi_P^{l,j}$) is defined as a continuous piecewise linear function with support $[\underline{x}_j^l, \hat{x}_{j,1}^l]$ (or $[\hat{x}_{j,P-1}^l, \bar{x}_j^l]$) and such that $\Psi_0^{l,j}(\underline{x}_j^l)=1$ (or $\Psi_P^{l,j}(\bar{x}_j^l)=1$). Unlike other networks, the P1-KAN layer, which is theoretically described as an operator from $\mathbb{R}^{d_0}$ to $\mathbb{R}^{d_1}$ by the equation (2), takes as input not only a sample $x \in \mathbb{R}^{d_0}$ but also the description of the support $(\underline{x}_j^l, \bar{x}_j^l)_{j=1,d_0}$.
In this version of the layer, the grid is uniform on $[\underline{x}_j^l, \bar{x}_j^l]$, and the vertices are generated for each direction j for $0 \le p \le P$ by

$$\hat{x}_{j,p}^l = \underline{x}_j^l + p\frac{\bar{x}_j^l - \underline{x}_j^l}{P}.$$

The operator estimating the value function associated to the layer on the hypercube G^l is given by:

$$\hat{\kappa}_{d_0,d_1}^{l,P}(x,G^l)_k = \sum_{j=1}^{d_0}\sum_{p=0}^{P} a_p^{l,k,j}\Psi_p^{l,j}(x_j), \text{ for } k=1,\dots,d_1. \tag{3}$$

The tensor $A_{d_0,d_1}^l = (a_p^{l,k,j})_{0\le p\le P, 1\le j\le d_0, 1\le k\le d_1}$ are the trainable variables of the network for layer l.
As output, the layer returns the values of $\hat{\kappa}_{d_0,d_1}^{l,P}(x,G^l)$ in $\mathbb{R}^{d_1}$ and the lattice $G^{l+1} = [\underline{G}^{l+1}, \bar{G}^{l+1}]$ obtained from the possible $\hat{\kappa}_{d_0,d_1}^{l,P}(x,G^l)$ values. Due to the use of the P_1 finite element approximation, this output lattice is exactly obtained from the A_{d_0,d_1}^l tensor by:

$$\underline{G}_k^{l+1} = \sum_{j=1}^{d_0} \min_{0\le p\le P} a_p^{l,k,j}$$
$$\bar{G}_k^{l+1} = \sum_{j=1}^{d_0} \max_{0\le p\le P} a_p^{l,k,j},$$

for $1 \leq k \leq d_1$.
Then the global layer as an operator from $\mathbb{R}^{d_0} \times \mathbb{R}^{d_0 \times 2}$ to $\mathbb{R}^{d_1} \times \mathbb{R}^{d_1 \times 2}$ is defined by:

$$\kappa^{l,P}_{d_0,d_1}(x, G^l) = (\hat{\kappa}^{l,P}_{d_0,d_1}(x, G^l), G^{l+1}). \tag{4}$$

2.1.2. *The P1-KAN Layer with an Adapting Lattice.*
In this version of the layer, the vertices in $]\underline{x}^l_j, \bar{x}^l_j[$ are initially generated randomly uniformly and their values are trained to adapt to the data. This is done by defining for $1 \leq p < P$ increasing values in $]0, 1[$ by $\frac{\sum_{k=1}^{p} e^k}{\sum_{k=1}^{P} e^k}$ where $e^1, \ldots, e^P$ are positive random variables. This set of values is then used to define the grid points in $]\underline{x}^l_j, \bar{x}^l_j[$ by an affine transformation.

In detail, the vertices in $]\underline{x}^l_j, \bar{x}^l_j[$ are generated for each direction j for $1 \leq p < P$ by

$$\hat{x}^l_{j,p} = \underline{x}^l_j + (\bar{x}^l_j - \underline{x}^l_j) \frac{\sum_{k=1}^{p} e^{y^{l,k,j}}}{\sum_{k=1}^{P} e^{y^{l,k,j}}},$$

where the matrix $Y^l_{d_0} = (y^{l,p,j})_{1 \leq p \leq P, 1 \leq j \leq d_0}$ has elements in $\mathbb{R}$. The tensor $A^l_{d_0,d_1} = (a^{l,k,j}_p)_{0 \leq p \leq P, 1 \leq j \leq d_0, 1 \leq k \leq d_1}$ and $Y^l_{d_0}$ are the trainable variables of the layer.

2.1.3. *Importance of Adaptation.* To illustrate the importance of adaptation, we minimize the mean squared error in one dimension of our P1-KAN layer approximation, denoted $f_P(x)$, with respect to the one-dimensional function $f(x) = x^8 1_{x<0.45} + (0.9 - x)^8 1_{x \geq 0.45}$ on $[0, 1]$ for different values of P. In Figure 2, we plot f_P, f and the vertices of the lattice with and without adaptation. As expected, adaptation increases the number of points in areas where the gradient is the highest (see remark 2.1). The mean squared error obtained after optimization is given in Table 1. The cost of a calculation using adaptation is less than twice the cost of a calculation without adaptation.

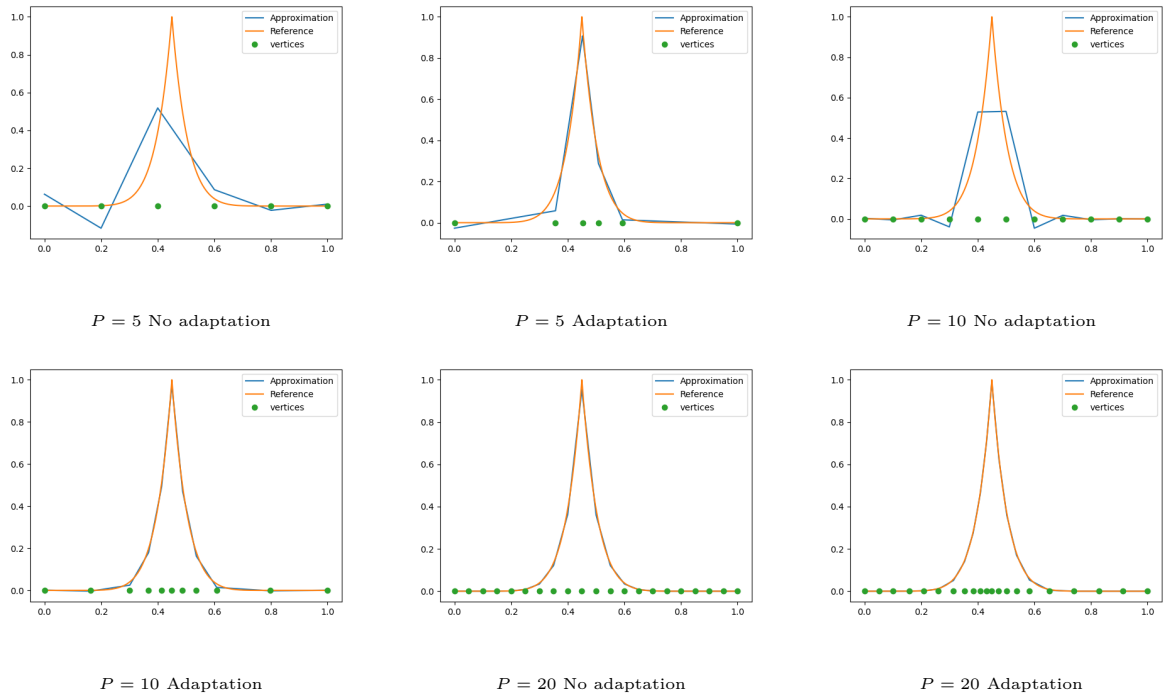

FIGURE 2. Reference function and approximation with or without adaptation. Vertices on the x-axis.

P	Error without adaptation	Error with adaptation
5	0.1545	0.00492
10	0.0737	3.55E-4
20	4.7E-4	5.22E-5

TABLE 1. Mean squared error.

2.2. **The Global P1-KAN Network.** As shown in the previous section, the P1-KAN layer inputs x values and a hypercube, and it outputs the values obtained by the operator and a hypercube. Therefore, it is natural to stack the layers without using any grid adaptation or sigmoid function to send the output of the layer back to a known bounded domain. The P1-KAN network takes as the initial hypercube used for the first layer the hypercube corresponding to the bounded domain where we want to approximate the unknown function. Supposing that the number of neurons is equal to N, the number of inside layers is L, the global operator for $x \in \mathbb{R}^n$ is

$$K(x) = \hat{\kappa}^{L,P}_{N,1} \circ \kappa^{L-1,P}_{N,N} \circ \ldots \circ \kappa^{0,P}_{n,N}(x, [0,1]^n), \tag{5}$$

where the $\kappa^{l,P}$ are defined in (4) , $\hat{\kappa}^{L,P}$ in (3) and the parameters to optimize are $\theta = \mathcal{A} := A^0_{n,N} \cup A^1_{N,N} \cup \ldots \cup A^L_{N,d}$ for the P1-KAN network without adaptation, and $\theta = \mathcal{A} \cup Y^0_n \cup Y^1_N \cup \ldots \cup Y^L_N$ for the P1-KAN

with adaptation.
The approximation space spanned by the P1-KAN parametrized by θ is then:

$$\mathcal{N}_n^{L,N,P} = \{f_\theta(x) = \hat{\kappa}_{N,1}^{L,P} \circ \kappa_{N,N}^{L-1,P} \circ \cdots \circ \kappa_{n,N}^{0,P}(x,[0,1]^n) \text{with } \theta \in \mathbb{R}^Q\},$$

where $Q = (P+1)(nN + (L-1)N^2 + N)$ for the P1-KAN without adaptation and $Q = (P+1)(nN + (L-1)N^2 + N) + (P-1)(n + LN)$ with adaptation.
An implementation in Pytorch is available at https://fime-lab.org/warin-xavier.

2.3. **Convergence theorems.** As the P1-KAN networks are based on a classical method in numerical analysis, an approximation error can be estimated.
Let us define the interpolation operator $\Pi_P^{[a,b]}$ of a function f defined on $[a,b] \subset \mathbb{R}$, with a step $h = \frac{b-a}{P}$ by

$$\Pi_P^{[a,b]}(f)(x) = \sum_{i=0}^{P} f(a+ih)\Psi_i(x),$$

where $\Psi_0(x) = \max(1 - \frac{x-a}{h}, 0)$, $\Psi_P(x) = \max(\frac{x-b+h}{h}, 0)$, and for $i = 1, \dots, P-1$,

$$\Psi_i(x) = \begin{cases} \frac{x-(a+(i-1)h)}{h} & x \in [a+(i-1)h, a+ih] \\ \frac{(a+(i+1)h)-x}{h} & x \in [a+ih, a+(i+1)h]. \end{cases}$$

For a set of Lipschitz functions $f_i : [0,1] \longrightarrow \mathbb{R}$ for $i = 1, \dots, n$, we denote

$$\begin{aligned} \mu(\{f_i\}_{i=1,n}) :=& [\underline{\mu}(\{f_i\}_{i=1,n}), \bar{\mu}(\{f_i\}_{i=1,n})] \\ :=& [\min_{x\in[0,1]^n} \sum_{i=1}^n f_i(x_i), \max_{x\in[0,1]^n} \sum_{i=1}^n f_i(x_i)], \end{aligned}$$

which is well defined by continuity on a compact.

Proposition 2.1. *Supposing that the $(\psi_i)_{i=1,\dots,2n+1}$ and the $(\Phi_{i,j})_{i=1,\dots,2n+1,j=1,\dots,n}$ in the Kolmogorov-Arnold expansion* (1) *are K-Lipschitz. For $h > 0$ given, let us define*

$$P = \lfloor \frac{1}{h} \rfloor + 1,$$

$$\hat{P}_i = \lfloor \frac{\bar{\mu}(\{\Pi^{[0,1]}(\Phi_{i,j})\}_{j=1,n}) - \underline{\mu}(\{\Pi^{[0,1]}(\Phi_{i,j})\}_{j=1,n})}{h} \rfloor + 1,$$

for $i = 1, \dots 2n+1$, then there exists a constant C such that

$$\sup_{x\in[0,1]^n} |f(x) - \sum_{i=1}^{2n+1} \Pi_{\hat{P}_i}^{\mu(\{\Pi_P^{[0,1]}(\Phi_{i,j})\}_{j=1,\dots,n})}(\psi_i)(\sum_{j=1}^n \Pi_P^{[0,1]}(\Phi_{i,j})(x_j))| \leq Ch.$$

Proof. By classical estimates on P_1 interpolation on Lipschitz functions, there exists D such that

$$\sup_{x\in[0,1]} |\Pi_P^{[0,1]}(\Phi_{i,j})(x) - \Phi_{i,j}(x)| \leq Dh. \tag{6}$$

Then

$$\begin{aligned}
A =& |f(x) - \sum_{i=1}^{2n+1} \Pi_{P_i}^{\mu(\{\Pi_P^{[0,1]}(\Phi_{i,j})\}_{j=1,\dots,n})}(\psi_i)(\sum_{j=1}^{n} \Pi_P^{[0,1]}(\Phi_{i,j})(x_j))| \\
\leq& |f(x) - \sum_{i=1}^{2n+1} \psi_i(\sum_{j=1}^{n} \Pi_P^{[0,1]}(\Phi_{i,j})(x_j))| + |\sum_{i=1}^{2n+1} (\psi_i - \Pi_{P_i}^{\mu(\{\Pi_P^{[0,1]}(\Phi_{i,j})\}_{j=1,\dots,n})}(\psi_i))(\sum_{j=1}^{n} \Pi_P^{[0,1]}(\Phi_{i,j})(x_j))| \\
\leq& K \sum_{i=1}^{2n+1} |\sum_{j=1}^{n} \Pi_P^{[0,1]}(\Phi_{i,j})(x_j) - \Phi_{i,j}(x_j)| + (2n+1)Dh \\
\leq& (2n+1)D(Kn+1)h.
\end{aligned}$$

using (6). □

Proposition 2.2. *Under the conditions of Proposition 2.1, the P1-KAN without adaptation defined by* (5) *with $L \geq 1$ and $N \geq 2n+1$ satisfies:*

$$\min_{g \in \mathcal{N}_{n,1}^{L,N}} \sup_{x \in [0,1]^d} |f(x) - g(x)| \leq ch.$$

Proof. As the identity and the zero functions can be generated by the functions $\Psi_p^{l,j}$ in (2),

$$\begin{aligned}
\min_{g \in \mathcal{N}_{n,d}^{L,N}} \sup_{x \in [0,1]^d} |f(x) - g(x)| \leq& \min_{g \in \mathcal{N}_{n,d}^{1,2n+1}} \sup_{x \in [0,1]^d} |f(x) - g(x)| \\
\leq& \sup_{x \in [0,1]^d} |f(x) - \sum_{i=1}^{2n+1} \Pi_{\hat{P}_i}^{\mu(\{\Pi_P^{[0,1]}(\Phi_{i,j})\}_{1,\dots,d})}(\psi_i)(\sum_{j=1}^{n} \Pi_P^{[0,1]}(\Phi_{i,j})(x_j))| \\
\leq& Ch,
\end{aligned}$$

by Proposition 2.1. □

These results can be extended to the case where the functions in the Kolmogorov expansion are more regular.

Proposition 2.3. *Suppose that the $(\psi_i)_{i=1,\dots,2n+1}$ and the $(\Phi_{i,j})_{i=1,\dots,2n+1,j=1,\dots,n}$ in the Kolmogorov-Arnold expansion* (1) *are C^1 with K-Lipschitz derivatives. The P1-KAN without adaptation defined by* (5) *with $L \geq 1$ and $N \geq 2n+1$ and a number of meshes defined by P and $\hat{P}_i$ for $i = 1, \dots, N$ as in Proposition 2.1, then there exists a constant C such that*

$$\min_{g \in \mathcal{N}_{m,d}^{L,N}} \sup_{x \in [0,1]^d} |f(x) - g(x)| \leq Ch^2.$$

Remark 2.1. *When the function to interpolate is, for example, C^1, the interpolation error is directly related to the maximum of its derivative (Theorem 7.2* [21]*). As a consequence, reducing the size of the mesh locally where the gradient is the highest allows us to achieve a smaller global error. This explains the behavior of the P1-KAN layer with adaptation in section 2.1.3.*

In the general case, where the Kolmogorov-Arnold expansion functions are not smooth, a universal approximation theorem is given:

Theorem 2.1. *The space spanned by $\mathcal{N}_n^{L,N,P}$ letting N vary for $L \geq 1$, $P > 1$ is dense in $C^0([0,1]^n)$ with the sup norm when adaptation is used.*

Proof. As usual, it is sufficient to show the result by fixing $P = 2$ and $L = 1$. Using [12], for all functions $f \in C^0([0,1]^n)$, there exist N, $A \in \mathbb{R}^N$, $B \in \mathbb{R}^{N\times n}$, $C \in \mathbb{R}^N$ such that:

$$\sup_{x\in[0,1]^n} |f(x) - \sum_{i=1}^{N} A_i \max(B_i x + C_i, 0)| \leq \epsilon,$$

where B_i is the row vector defined by $(B_{i,j})_{j=1,n}$. It is clear that one can find $\hat{\kappa}^{0,2}_{n,N}$ defined by (3) such that $\hat{\kappa}^{0,2}_{n,N}(x,[0,1]^n)_i = B_i x + C_i$ for $i = 1,\dots,N$. For each i on $G^1_i = [\inf_{x\in[0,1]^n} B_i x + C_i, \sup_{x\in[0,1]^n} B_i x + C_i]$, $g_i(x) = A_i \mathrm{ReLU}(x)$ is either linear, or $0 \in G^{1^{\mathrm{o}}}_i$ so $g_i(x)$ can be generated by a $\hat{\kappa}^{1,2}_{N,1}(x, G^1)_i$ using adaptation so that $\hat{x}^1_{i,1} = 0$ when $0 \in G^{1^{\mathrm{o}}}_i$. □

When adaptation is not used, the ReLU function cannot directly be generated as 0 is generally not in the lattice. The ReLU function is therefore uniformly approximated by piecewise linear functions by increasing P, which gives the second theorem:

Theorem 2.2. *The space spanned by $\mathcal{N}^{L,N,P}_n$ letting N and P vary for $L \geq 1$ is dense in $C^0([0,1]^n)$ with the sup norm when adaptation is not used.*

3. Numerical Results for Function Approximation

In this section, we compare the classical feedforward network with Spline-KAN [18], Fast-KAN [17], ReLU-KAN [17], and P1-KAN for the approximation of two types of functions defined on $[0,1]^n$.

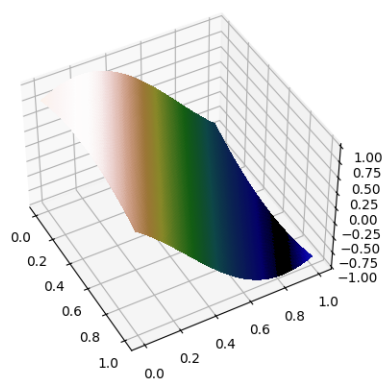

Figure 3. Function A in 2D.

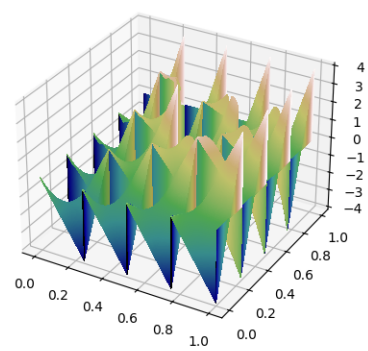

Figure 4. Function B in 2D.

A The first function is smooth but very fast oscillating with increasing dimension and is defined for $x \in [0,1]^n$ by:

$$f(x) = \cos\left(\sum_{i=1}^{n} i y_i\right),$$

where $y = 0.5 + \frac{2x-1}{\sqrt{n}}$. The function in 2D is shown in Figure 3.

B The second function is very irregular and is given as

$$f(x) = n\left(\prod_{i=1}^{n} y_i + 2\left(4\prod_{i=1}^{n} x_i - \lfloor 4\prod_{i=1}^{n} x_i \rfloor\right) - 1\right),$$

where $y := 2\,(4x - \lfloor 4x \rfloor) - 1$ and for $x \in \mathbb{R}^n$, $\lfloor x \rfloor := (\lfloor x_i \rfloor)_{i=1,n}$. The function is shown in 2D in Figure 4.

To approximate a function f with a neural network κ, we use the classical quadratic loss function defined as:

$$L = \mathbb{E}[(f(X) - \kappa(X))^2],$$

where X is a uniform random variable on $[0,1]^n$. Using a stochastic gradient algorithm with the ADAM optimizer, a learning rate of 10^{-3}, and a batch size of 1000, we minimize the loss L. The MLPs use a ReLU activation function, with either 2 layers with 10, 20, 40 neurons for each layer or 3 layers with 10, 20, 40, 80, 160 neurons: In each case, the MLPs are optimized by varying the number of neurons and layers, and only the result that gives the smallest loss during the iterations is kept for the plots. The different KAN networks are compared using the same parametrization (number of hidden layers, number of neurons, number of meshes used for the 1D functions). The ReLU-KAN has an additional parameter k, which we keep at 3 as suggested in the original article. For all plots, every 100 gradient iterations, the loss is calculated more accurately using 10^5 samples, giving a series of log-losses plotted using a moving average window of 10 results.
ReLU-KAN is very efficient in terms of computation time as it can be broken down into a few operations involving only the ReLU function, matrix addition, and multiplication. On an 11th generation Intel(R) Core(TM) i7-11850H @ 2.50GHz, using the same parametrization of the KAN nets, the P1-KAN with adaptation computation time is between 1.5 and 2 times slower than the ReLU-KAN, while the P1-KAN without adaptation gives similar computing times. For the spline version of the KAN originally from [18], we use the efficient Pytorch KAN implementation. For the Fast-KAN [17], we use the Pytorch implementation.

3.1. **Results for the A Function.** The results in dimension 6 shown in Figure 5 on a single run seem to indicate that the original Spline-KAN network converges faster than the P1-KAN network with adaptation, which is the second most effective network. In general, the ReLU-KAN network converges at least as well as the best feedforward network, while the Fast-KAN is the least effective network. The P1-KAN without adaptation is less effective than the P1-KAN with adaptation.

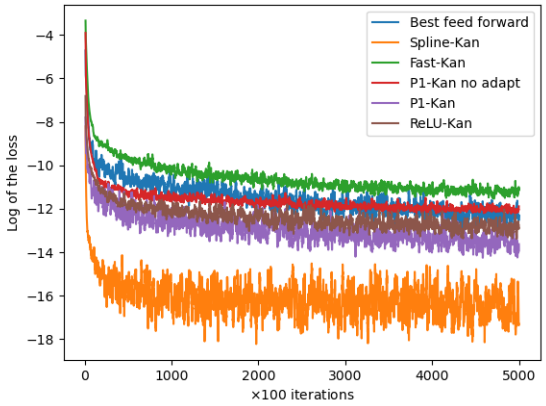

2 hidden layers of 10 neurons, $P = 5$.

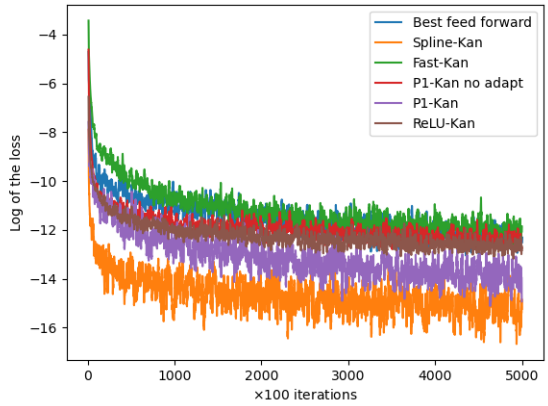

3 hidden layers of 10 neurons, $P = 5$.

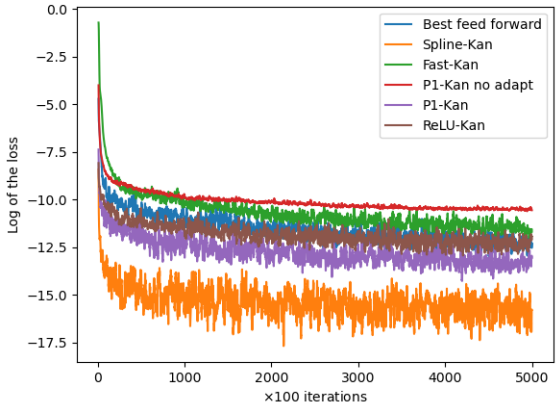

2 hidden layers of 10 neurons, $P = 10$.

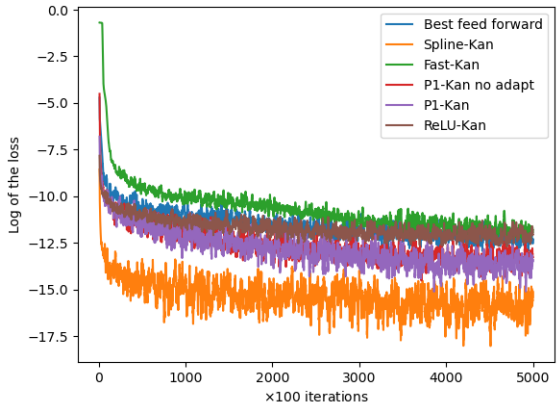

3 hidden layers of 10 neurons, $P = 10$.

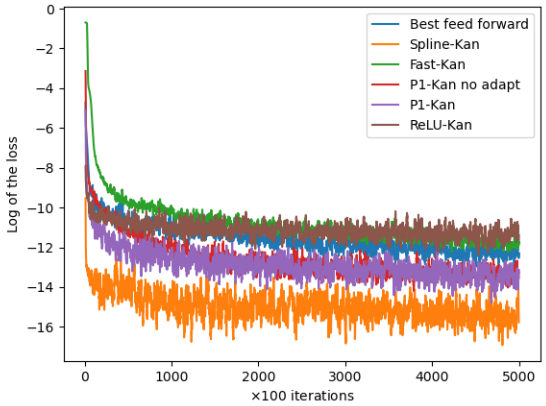

2 hidden layers of 10 neurons, $P = 20$.

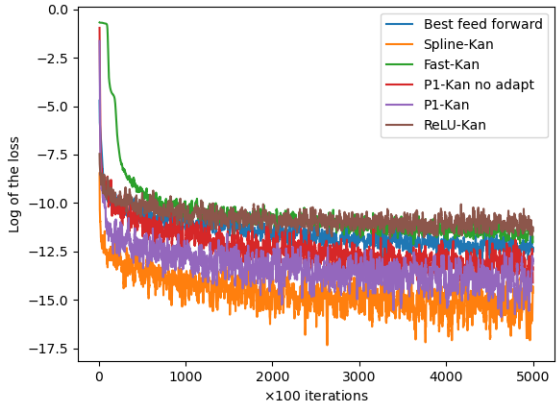

3 hidden layers of 10 neurons, $P = 20$.

FIGURE 5. Results in dimension 6 for function A.

In dimension 12, as shown in Figure 6, the Spline-KAN and the P1-KAN with adaptation again give the best results. The Fast-KAN and the ReLU-KAN fail, while the feedforward network seems to converge very slowly and its accuracy remains limited. Notice that the P1-KANs give good results when P is small, but do not give any results when P is too large. Again, adaptation of the P1-KAN gives far better results.

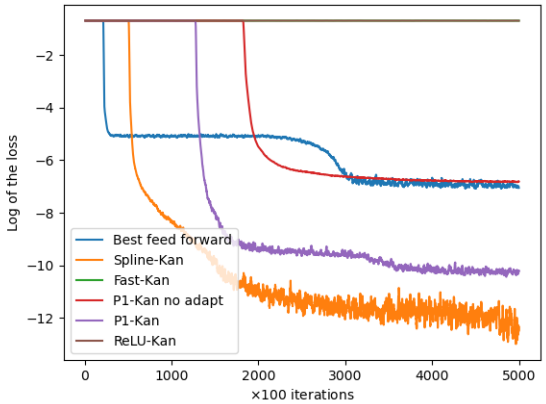

2 hidden layers of 10 neurons, $P = 5$.

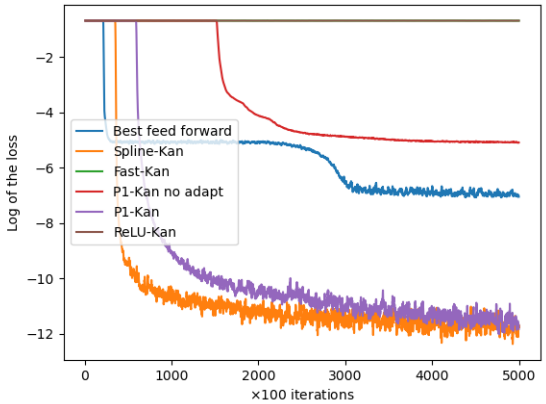

3 hidden layers of 10 neurons, $P = 5$.

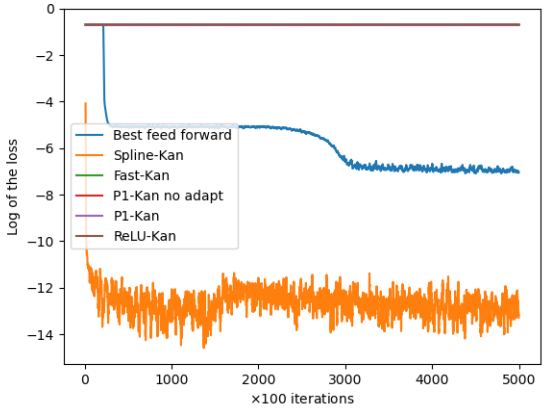

2 hidden layers of 10 neurons, $P = 10$.

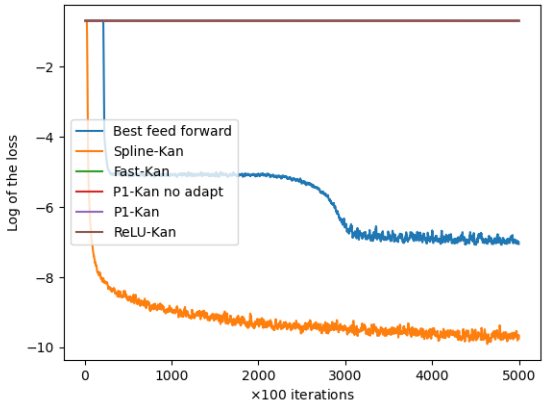

3 hidden layers of 10 neurons, $P = 10$.

FIGURE 6. Results in dimension 12 for function A.

As these graphs are obtained with one run, we provide in Table 2 the average results and standard deviation obtained from 10 runs of the P1-KANs and the Spline-KAN. The best results obtained by the P1-KAN with adaptation and the Spline-KAN are very similar. The Spline-KAN allows the use of higher P values.

Method	Number of Layers	Number of Neurons	P	Average	Std
Spline-KAN	2	10	5	6.31E-03	1.84E-02
Spline-KAN	2	10	10	3.95E-03	8.59E-03
Spline-KAN	2	10	20	5.08E-04	4.69E-04
Spline-KAN	3	10	5	2.50E-04	2.81E-04
Spline-KAN	3	10	10	1.55E-03	2.04E-03
Spline-KAN	3	10	20	5.00E-01	1.50E+00
P1-KAN no adapt	2	10	5	1.80E-01	2.17E-01
P1-KAN no adapt	2	10	10	4.50E+00	1.49E+00
P1-KAN no adapt	2	10	20	5.00E+00	7.51E-03
P1-KAN no adapt	3	10	5	2.70E-02	2.25E-02
P1-KAN no adapt	3	10	10	4.51E+00	1.49E+00
P1-KAN no adapt	3	10	20	5.00E+00	5.38E-03
P1-KAN	2	10	5	1.75E-03	2.15E-03
P1-KAN	2	10	10	4.00E+00	2.00E+00
P1-KAN	2	10	20	5.00E+00	1.62E-02
P1-KAN	3	10	5	2.33E-04	1.34E-04
P1-KAN	3	10	10	3.50E+00	2.29E+00
P1-KAN	3	10	20	5.00E+00	1.15E-02

TABLE 2. Results obtained from 10 runs of the Spline-KAN and P1-KAN networks (with and without adaptation) in dimension 12: Average value and standard deviation obtained are given.

3.2. **Results for the B Function.** In dimension 2, as shown in Figure 7, we see that the feedforward network lags behind the KAN networks. By taking high values of P, the P1-KAN network is the only network that gives very good results. The Spline-KAN is the second-best network.

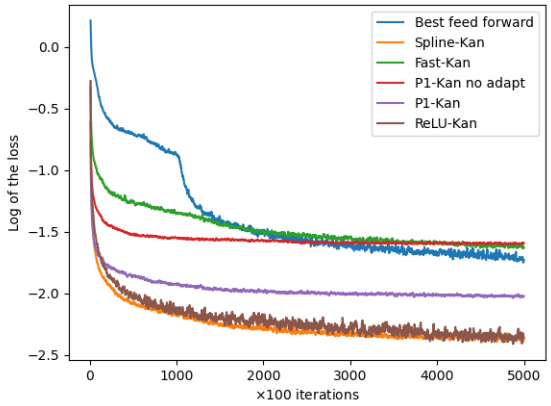

2 hidden layers of 10 neurons, $P = 5$.

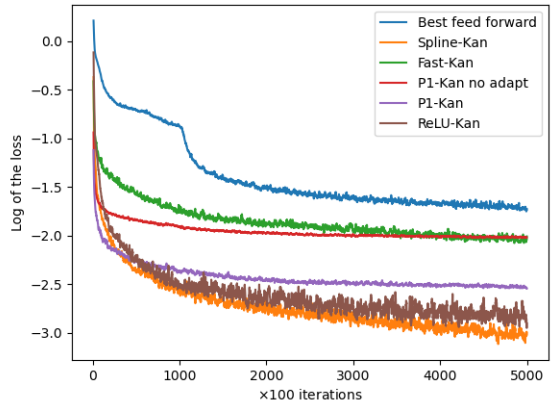

3 hidden layers of 10 neurons, $P = 5$.

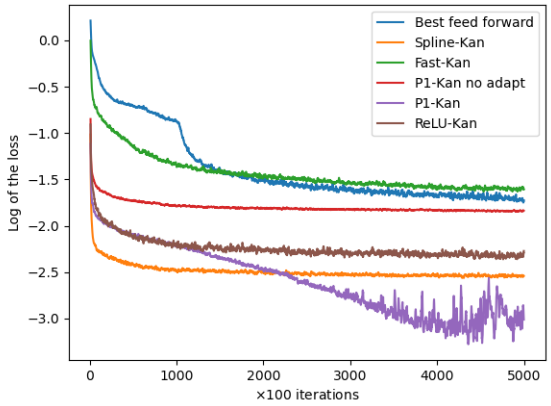

2 hidden layers of 10 neurons, $P = 10$.

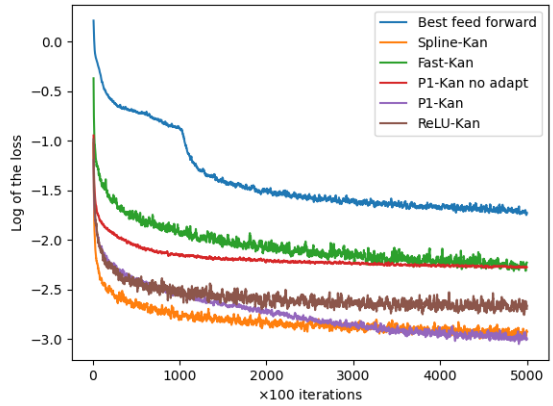

3 hidden layers of 10 neurons, $P = 10$.

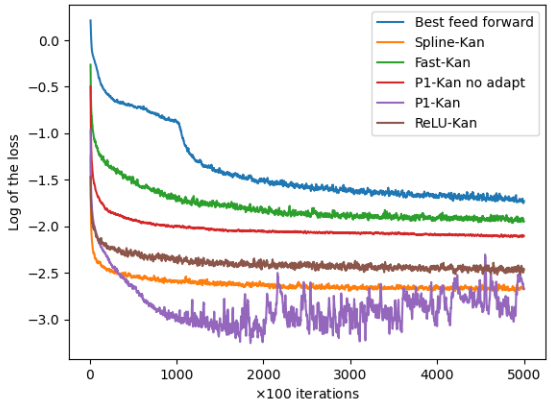

2 hidden layers of 10 neurons, $P = 20$.

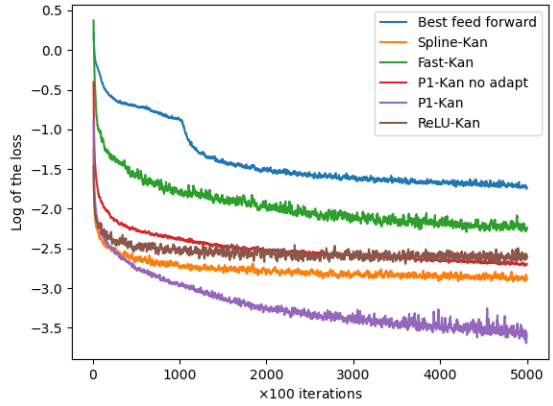

3 hidden layers of 10 neurons, $P = 20$.

FIGURE 7. Results in dimension 2 for function B.

Finally, if we go up to dimension 5, we see that the ReLU-KAN network can diverge. The P1-KAN network is the only one that gives acceptable results by using 2 or 3 hidden layers of 10 neurons and $P = 20$.

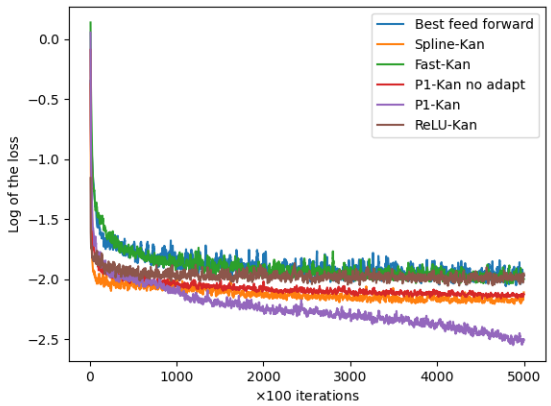

2 hidden layers of 10 neurons, $P = 10$

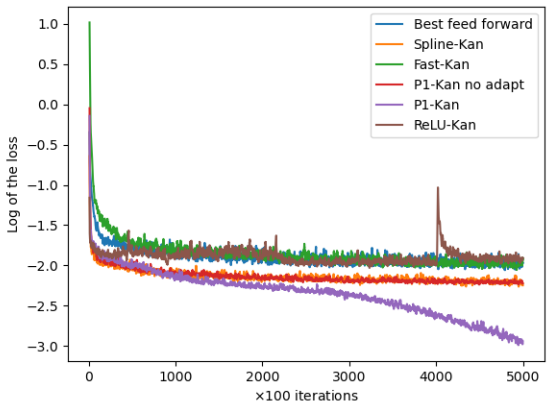

3 hidden layers of 10 neurons, $P = 10$

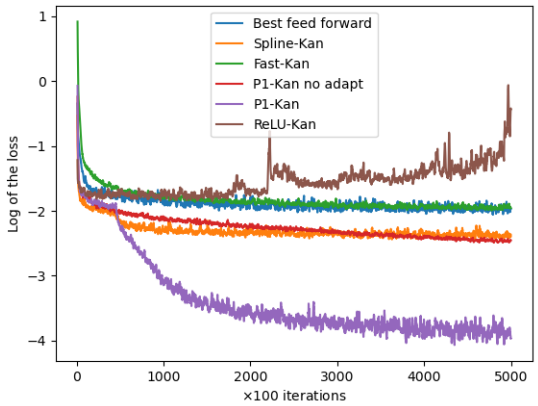

2 hidden layers of 10 neurons, $P = 20$

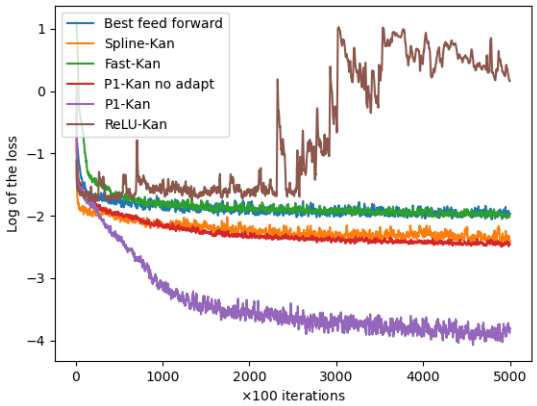

3 hidden layers of 10 neurons, $P = 20$

FIGURE 8. Results in dimension 5 for function B

Results in Table 3 indicate that P1-KAN with adaptation is far better than the two other KANs. The Spline-KAN and the P1-KAN without adaptation give similar results in this case.

Method	Number of Layers	Number of Neurons	P	Average	Std
Spline-KAN	2	10	5	1.16E+00	6.13E-02
Spline-KAN	2	10	20	9.12E-01	1.06E-01
Spline-KAN	3	10	5	1.17E+00	5.92E-02
Spline-KAN	3	10	10	1.07E+00	8.43E-02
Spline-KAN	3	10	20	8.65E-01	9.93E-02
P1-KAN no adapt	2	10	5	1.27E+00	3.06E-02
P1-KAN no adapt	2	10	20	1.01E+00	9.51E-02
P1-KAN no adapt	3	10	5	1.20E+00	2.74E-02
P1-KAN no adapt	3	10	10	1.10E+00	4.13E-02
P1-KAN no adapt	3	10	20	8.50E-01	5.40E-02
P1-KAN	2	10	5	1.25E+00	6.52E-02
P1-KAN	2	10	20	2.58E-01	8.04E-02
P1-KAN	3	10	5	1.23E+00	6.90E-02
P1-KAN	3	10	10	9.94E-01	2.15E-01
P1-KAN	3	10	20	2.12E-01	2.61E-02

TABLE 3. Results obtained from 10 runs of the Spline-KAN and P1-KAN networks in dimension 5: Average value and standard deviation obtained are given for the irregular case.

4. Application to Hydraulic Valley Optimization

Hydraulic valley optimization in countries with large valleys, such as France, Brazil, or Norway, is traditionally achieved using methods based on dynamic programming [2]. The objective to be maximized is the profit obtained by selling the electricity produced by the turbines of some interconnected reservoirs. These profits are therefore linked to some price scenarios, and the different reservoirs and turbines have to respect some constraints, either physical (size of the lake, availability of the turbines, etc.) or environmental (minimum flooding for fish, agriculture, minimum lake level for leisure activities, etc.), while facing the uncertainties linked to the inflows.
The optimization step is generally the week, i.e., for each hour of a week, anticipative controls are computed, assuming that all uncertainties (inflows, prices) are known at the beginning of the week. Using dynamic programming type methods, Bellman values are computed at the beginning of each week, maximizing the gain in expectation. Here, we test neural networks by comparing the results obtained with those obtained using traditional methods in production.

We suppose here that decisions are taken every week to turbine water using production units. During week $i \in [1, 52]$, time is discretized with three time steps per day. At the beginning of the week, turbining decisions are taken for each unit for each time step $t_{i,j}$, for $j = 0, \dots, 20$ according to a flow equation given in Section 4.1. We take the convention $t_i = t_{i,0}$. The energy generated and the function to maximize are given in Section 4.2.

4.1. The Flow Equation During a Week.

We suppose that the valley is composed of $\hat{N}$ reservoirs and $\tilde{N}$ is the number of production units operating. A production unit l of a reservoir m is numbered $U^{l,m}$ for $l = 1, \dots, \tilde{N}(l)$. Therefore $\tilde{N}(l)$ is the number of production units of the reservoir l.
A reservoir r receives water:

- due to inflow I^r (rain, uncontrolled rivers, etc.),

- from one of the $N^u(r)$ upstream controlled reservoirs: either because an upstream reservoir is overflowing, or because a production unit number $U^{l,m}$ associated with an upstream reservoir l is operating. $w(r,k)$ for $k = 1, \dots, N^u(r)$ is the number of the kth reservoir above reservoir r.

A reservoir releases water into one of its downstream reservoirs:

- when it is overflowing,
- when one of its production units $U^{r,m}$ is activated to generate power, releasing water to another reservoir.

The flow equation for the volume $\tilde{V}^r_{i,j+1}$ of a reservoir r is given in week i at time $t_{i,j+1}$ from the volume $V^r_{i,j}$ at the previous date without taking into account the overflow by:

$$\tilde{V}^r_{i,j+1} = V^r_{i,j} + I^r_{i,j} + \sum_{k=1}^{N^u(r)} \big(O^{w(r,k)}_{i,j} + \sum_{l=1}^{\tilde{N}(w(r,k))} T^{U^{w(r,k),l}}_{i,j} \Delta_{i,j} \big) - \sum_{k=1}^{\tilde{N}(r)} T^{U^{r,k}}_{i,j} \Delta_{i,j}$$

where:

- $\Delta_{i,j} = t_{i,j+1} - t_{i,j}$ is the time step,
- $O^k_{i,j}$ is the volume of water overflowed by the upstream lake k,
- $T^k_{i,j}$ is the water turbined from the production unit k per time unit.

The reservoir r has a primary constraint that cannot be violated: $0 \leq V^r_{i,j} \leq \bar{V}^r$ for all i, j and the volume of water overflowed satisfies $O^r_{i,j} = (\tilde{V}^r_{i,j+1} - \bar{V}^r)^+$, so that

$$V^r_{i,j+1} = \min(\tilde{V}^r_{i,j+1}, \bar{V}^r).$$

Environmental constraints are added but can be violated:

- $\underline{W}^r_{i,j} \leq V^r_{i,j} \leq \bar{W}^r_{i,j}$, for all i, j where $\underline{W}^r$ and $\bar{W}^r$ are given,
- $\underline{T}^k_{i,j} \leq T^k_{i,j}$ where $\underline{T}^k$ is also given for each production unit k.

Moreover, the maximum turbining for a production unit k associated with a reservoir r is a function of the water level in the reservoir r, giving the constraints that cannot be violated:

$$T^k_{i,j} \leq \bar{T}^k(V^r_{i,j}),$$

where $\bar{T}^k$ are given functions associated with the production unit.

4.2. **Expected Gain to Maximize.** We denote $T = (T^k_{i,j})_{i=1,\dots 52, j=0\dots 20, k=1,\dots,\tilde{N}}$ where the $T^k_{i,j}$ are functions of the available information at the beginning of week i, assuming that the $(I^r_{i,j})_{j=0,20,r=1,\dots,\hat{N}}$, $(S_{t_{i,j}})_{j=0,20}$ are known. Each production unit k associated with lake r transforms the volume turbined T per unit time into power by a function $\phi^k(T, V^r)$ which is an increasing function of the level of the reservoir.
The expected gain is given by selling the electricity at a price S_t and the function to maximize is given over 52 weeks by:

$$J(T) = G(T) - \epsilon \xi(T),$$

with the gain given as

$$G(T) = \sum_{r=1}^{\hat{N}} \sum_{k=1}^{\tilde{N}(r)} \sum_{i=1}^{52} \sum_{j=0}^{20} \mathbb{E}[S_{t_{i,j}} \phi^{U^{r,k}}(T^{U^{r,k}}_{i,j}, V^r_{i,j}) \Delta_{i,j}],$$

the volume violated by

$$\xi(T) = \sum_{r=1}^{\hat{N}} \sum_{i=1}^{52} \sum_{j=0}^{20} \left(\mathbb{E}[(\underline{W}_{i,j}^r - V_{i,j}^r)^+ + (V_{i,j}^r - \bar{W}_{i,j}^r)^+] + \Delta_{i,j} \sum_{k=1}^{\tilde{N}(r)} \mathbb{E}[(\underline{T}_{i,j}^{U^{r,k}} - T_{i,j}^{U^{r,k}})^+] \right)$$

where ϵ is a penalty factor.

4.3. **Parametrization of the Neural Networks.** We use 52 neural networks ϕ parametrized by $(\theta_i)_{i=1,\dots,52}$ for the problem (one per week). As input for the network i corresponding to week i, we take:

- the volume of each lake $V = (V_{i,0}^k)_{k=1,\dots,\hat{N}}$ at the beginning of the week (at date $t_{i,0}$),
- an inflow scenario for week i for all the reservoirs: $I = (I_{i,j}^k)_{j=0,\dots,20,k=1,\dots,\hat{N}}$,
- a price scenario for week i: $S = (S_{t_{i,j}})_{j=0,\dots,20}$.

Using a sigmoid function as the activation function for the output layer, the neural network outputs $\phi^{\theta_i}(V, I, S) \in [0,1]^{\tilde{N} \times 20}$. As in [27], the turbining control of each production unit at each date $t_{i,j}$, $j = 0, \dots, 20$ is obtained from its maximum allowed $(\bar{T}_{i,j}^k(V_{i,j}^r))_{j=0,\dots,20,k=1,\dots,\tilde{N}}$ by

$$\tilde{T}_{i,j}^{\theta_i,k} = \bar{T}_{i,j}^k(V_{i,j}^r)\phi^{\theta_i}(V, I, S)_{k,j}, \text{ for } i = 1, \dots, 52, \quad j = 0, \dots, 20, \quad k = 1, \dots, \tilde{N}.$$

Setting $\tilde{T}^\theta = (\tilde{T}_{i,j}^{\theta_i,k})_{i=1,\dots,52,j=0,\dots,20,k=1,\dots,\tilde{N}}$, $\theta = (\theta_i)_{i=1,\dots,52}$, we are left to calculate

$$\theta^* = \operatorname*{argmax}_\theta G(\tilde{T}^\theta) - \epsilon\xi(\tilde{T}^\theta). \tag{7}$$

We take $\epsilon = 5 \times 10^{-3}$. Classically, we solve (7) using the Adam stochastic gradient algorithm with a learning rate equal to 10^{-3}. The batch size is taken equal to 2000. The number of inflow scenarios is limited (equal to 42) and a scenario generator allows us to build as many scenarios as we wish to avoid over-fitting. Price scenarios are generated by a software calculating marginal prices associated with the global electrical network. The MLP uses the GeLU activation function [11] which seems to give slightly better results than the ReLU function. The P1-KAN network with adaptation is used.

4.4. **The Test Case and the Results.** The structure of the valley is given in Figure 9: the green squares represent the reservoirs while the yellow circles represent the production units. This valley is hard to optimize with classical methods based on dynamic programming due to its characteristics.

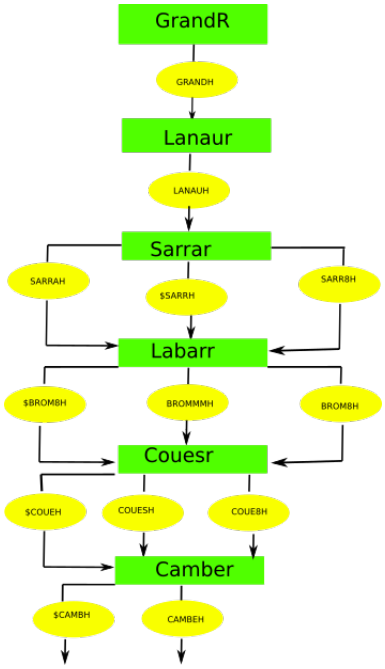

FIGURE 9. Structure of the valley

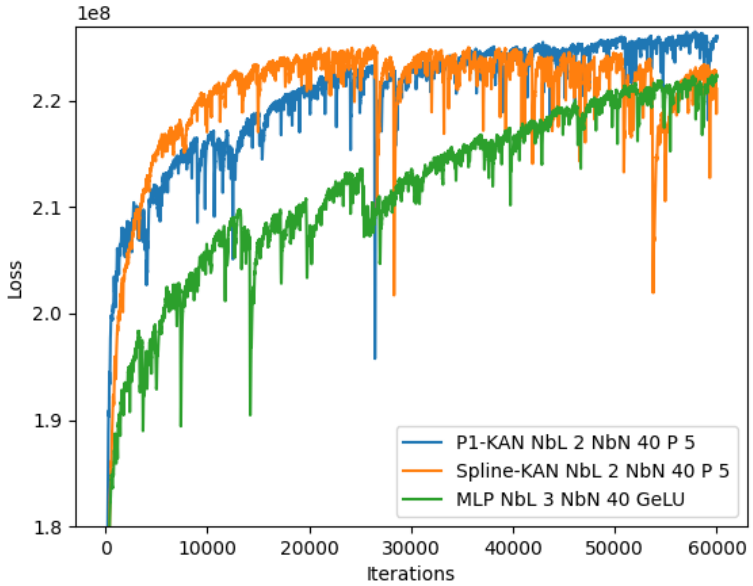

FIGURE 10. Convergence (NbL: number of layers, NbN: number of neurons)

Using 60,000 gradient iterations and a rolling window of 50 successive results, the convergence plot in Figure 10 indicates that the Spline-KAN and P1-KAN networks converge faster than the MPL, but the P1-KAN optimizes better. The MLP seems to be able to get a result better than the Spline-KAN. The iteration time is very similar on the NVIDIA H100 GPU for the different architectures: most of the computation is not related to the evaluation of the control by the networks.

The software in production, based on dynamic programming (DP), uses linear programming resolution to solve transition problems during the week (see Chapter 6 [9] for a description of the resolution using Bellman cuts). It only sees the historical inflows (duplicated three times) and 126 price scenarios. Penalties are tuned and settled specifically depending on the type of constraint violation. In Table 4, we present the gain function obtained and the volume of constraint violations with the scenarios used in production.

Method	G	ξ
DP	209.6	1198
P1-KAN	208.2	661
Spline-KAN	207.3	680
MLP GeLU	205.7	800

TABLE 4. Expected gains G in millions of Euros, and violations in $10^6 m^3$.

The approach using neural networks is far more robust as it is obtained using far more scenarios. Gains are very slightly below those obtained by the software in production, but the constraints are much less violated.

As the optimization by the software in production only takes two hours on fewer than 10 CPUs, the approach using machine learning, which takes two weeks to train, is not competitive but provides a reference and allows us to address some constraints that are impossible to handle with dynamic programming methods.

5. Conclusion

The P1-KAN is an excellent network with proven convergence properties for approximating functions. When the function to be approximated is smooth, it gives similar results to the Spline-KAN, but it is most effective when the function to be approximated is irregular. Using different networks in stochastic optimization on a real case, results confirm that the P1-KAN with adaptation leads to the most effective approach.

References

[1] Diab W Abueidda, Panos Pantidis, and Mostafa E Mobasher. Deepokan: Deep operator network based on kolmogorov arnold networks for mechanics problems. *arXiv preprint arXiv:2405.19143*, 2024.

[2] Richard Bellman. Dynamic programming and stochastic control processes. *Information and control*, 1(3):228–239, 1958.

[3] Alexander Dylan Bodner, Antonio Santiago Tepsich, Jack Natan Spolski, and Santiago Pourteau. Convolutional kolmogorov-arnold networks. *arXiv preprint arXiv:2406.13155*, 2024.

[4] Zavareh Bozorgasl and Hao Chen. Wav-kan: Wavelet kolmogorov-arnold networks. *arXiv preprint arXiv:2405.12832*, 2024.

[5] Arindam Chaudhuri. B-splines. *arXiv preprint arXiv:2108.06617*, 2021.

[6] Minjong Cheon. Demonstrating the efficacy of kolmogorov-arnold networks in vision tasks. *arXiv preprint arXiv:2406.14916*, 2024.

[7] Remi Genet and Hugo Inzirillo. Tkan: Temporal kolmogorov-arnold networks. *arXiv preprint arXiv:2405.07344*, 2024.

[8] Maximilien Germain, Huyên Pham, Xavier Warin, et al. Neural networks-based algorithms for stochastic control and pdes in finance. *arXiv preprint arXiv:2101.08068*, 2021.

[9] Hugo Gevret, Nicolas Langrené, Jerome Lelong, Rafael D Lobato, Thomas Ouillon, Xavier Warin, and Aditya Maheshwari. *STochastic OPTimization library in C++*. PhD thesis, EDF Lab, 2018.

[10] Federico Girosi and Tomaso Poggio. Representation properties of networks: Kolmogorov's theorem is irrelevant. *Neural Computation*, 1(4):465–469, 1989.

[11] Dan Hendrycks and Kevin Gimpel. Gaussian error linear units (gelus). *arXiv preprint arXiv:1606.08415*, 2016.

[12] Kurt Hornik, Maxwell Stinchcombe, and Halbert White. Universal approximation of an unknown mapping and its derivatives using multilayer feedforward networks. *Neural networks*, 3(5):551–560, 1990.

[13] William Knottenbelt, Zeyu Gao, Rebecca Wray, Woody Zhidong Zhang, Jiashuai Liu, and Mireia Crispin-Ortuzar. Coxkan: Kolmogorov-arnold networks for interpretable, high-performance survival analysis. *arXiv preprint arXiv:2409.04290*, 2024.

[14] Andrei Nikolaevich Kolmogorov. *On the representation of continuous functions of several variables by superpositions of continuous functions of a smaller number of variables*. American Mathematical Society, 1961.

[15] Tran Xuan Hieu Le, Thi Diem Tran, Hoai Luan Pham, Vu Trung Duong Le, Tuan Hai Vu, Van Tinh Nguyen, Yasuhiko Nakashima, et al. Exploring the limitations of kolmogorov-arnold networks in classification: Insights to software training and hardware implementation. *arXiv preprint arXiv:2407.17790*, 2024.

[16] Chenxin Li, Xinyu Liu, Wuyang Li, Cheng Wang, Hengyu Liu, and Yixuan Yuan. U-kan makes strong backbone for medical image segmentation and generation. *arXiv preprint arXiv:2406.02918*, 2024.

[17] Ziyao Li. Kolmogorov-arnold networks are radial basis function networks. 2024.

[18] Ziming Liu, Yixuan Wang, Sachin Vaidya, Fabian Ruehle, James Halverson, Marin Soljačić, Thomas Y Hou, and Max Tegmark. Kan: Kolmogorov-arnold networks. *arXiv preprint arXiv:2404.19756*, 2024.

[19] Tomaso Poggio, Andrzej Banburski, and Qianli Liao. Theoretical issues in deep networks. *Proceedings of the National Academy of Sciences*, 117(48):30039–30045, 2020.

[20] Qi Qiu, Tao Zhu, Helin Gong, Liming Chen, and Huansheng Ning. Relu-kan: New kolmogorov-arnold networks that only need matrix addition, dot multiplication, and relu. *arXiv preprint arXiv:2406.02075*, 2024.

[21] Alfio Maria Quarteroni, Riccardo Sacco, and Fausto Saleri. *Méthodes Numériques: Algorithmes, analyse et applications*. Springer Science & Business Media, 2007.

[22] Haoran Shen, Chen Zeng, Jiahui Wang, and Qiao Wang. Reduced effectiveness of kolmogorov-arnold networks on functions with noise. *arXiv preprint arXiv:2407.14882*, 2024.

[23] Chi Chiu So and Siu Pang Yung. Higher-order-relu-kans (hrkans) for solving physics-informed neural networks (pinns) more accurately, robustly and faster. *arXiv preprint arXiv:2409.14248*, 2024.

[24] Sidharth SS. Chebyshev polynomial-based kolmogorov-arnold networks: An efficient architecture for nonlinear function approximation. *arXiv preprint arXiv:2405.07200*, 2024.

[25] Hoang-Thang Ta. Bsrbf-kan: A combination of b-splines and radial basic functions in kolmogorov-arnold networks. *arXiv preprint arXiv:2406.11173*, 2024.

[26] Cristian J Vaca-Rubio, Luis Blanco, Roberto Pereira, and Màrius Caus. Kolmogorov-arnold networks (kans) for time series analysis. *arXiv preprint arXiv:2405.08790*, 2024.

[27] Xavier Warin. Reservoir optimization and machine learning methods. *EURO Journal on Computational Optimization*, 11:100068, 2023.

[28] Jinfeng Xu, Zheyu Chen, Jinze Li, Shuo Yang, Wei Wang, Xiping Hu, and Edith C-H Ngai. Fourierkan-gcf: Fourier kolmogorov-arnold network–an effective and efficient feature transformation for graph collaborative filtering. *arXiv preprint arXiv:2406.01034*, 2024.

[29] Xingyi Yang and Xinchao Wang. Kolmogorov-arnold transformer. *arXiv preprint arXiv:2409.10594*, 2024.

[30] Runpeng Yu, Weihao Yu, and Xinchao Wang. Kan or mlp: A fairer comparison. *arXiv preprint arXiv:2407.16674*, 2024.

Xavier Warin, EDF Lab Paris-Saclay and FiMe, Laboratoire de Finance des Marchés de l'Energie, 91120 Palaiseau, France
Email address: xavier.warin@edf.fr